Probability of spin-orbit torque driven magnetization switching assisted by spin-transfer torque
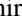
Tomohiro Taniguchi [1,*] Shinji Isogami,[2] Shuji Okame,[3] Katsuyuki Nakada,[3] Eiji Komura,[3] Tomoyuki Sasaki,[3] Seiji Mitani,[2] and Masamitsu Hayashi[2,4]

[1]*National Institute of Advanced Industrial Science and Technology, Research Center for Emerging Computing Technologies, Tsukuba, Ibaraki 305-8568, Japan*

[2]*National Institute for Materials Science, Tsukuba 305-0047, Japan,*

[3]*Advanced Products Development Center, Technology & Intellectual Property HQ, TDK Corporation, Ichikawa, Chiba 272-8558, Japan*

[4]*Department of Physics, The University of Tokyo, Tokyo 113-8654, Japan*

Spin-orbit torque (SOT) driven magnetization switching, assisted by spin-transfer torque (STT), enables field-free switching in ferromagnetic nanostructures and is expected to be a writing method for next-generation spintronic nonvolatile memory. The role of STT is to shift the magnetization pointing in an in-plane direction via the SOT to a different direction and ensure the switching. Here, we study the dependence of the switching probability on the STT strength using a numerical simulation of the Landau-Lifshitz-Gilbert (LLG) equation. While a monotonic increase of the switching probability with increasing STT strength is found in a relatively weak STT region, we find an unexpected increase in the error rate in a relatively large STT current close to a critical current. Based on the statistical analysis of the magnetization dynamics and solving the LLG equation analytically, we reveal that the origin of the switching error is the presence of an inactive region in the Bloch sphere where the magnetization dynamics becomes very slow compared with conventional SOT switching. Since this region exists far away from the initial state of the magnetization, a strong STT is necessary to reach the region. Accordingly, the switching error increases in a strong STT region. We also show that the issue can be solved by reducing the time only the STT is applied and/or enhancing the SOT strength.

I. INTRODUCTION

Spin-orbit torque (SOT) driven magnetization switching in a perpendicularly magnetized ferromagnet has been extensively studied from the viewpoints of both fundamental interest in spin-orbit interaction in solids and practical applications for three-terminal nonvolatile magnetic memory [1–9]. The SOT originates from spin-current injection into a ferromagnetic free layer from a heavy metal based bottom electrode by the spin Hall effect, in which a strong spin-orbit interaction in the heavy metal causes spin-dependent scattering and generates the spin current. The SOT drives a fast magnetization dynamics, on the order of nanoseconds, in the perpendicularly magnetized system and therefore is suitable as an ultrafast writing method for the magnetic memory. However, a central issue is that the magnetization switching requires some assistance for a deterministic switching. This is because the direction of the SOT is geometrically restricted to an in-plane direction, and thus, the SOT cannot determine the switching direction of the magnetization deterministically; thus, the switching will be probabilistic. Applying an external magnetic field along the current direction is a solution to achieve the deterministic switching. However, it is not preferable from the viewpoint of practical applications to use an external magnetic field. To overcome this issue and realize

field-free switching, several proposals have been made, such as utilizing lateral structure asymmetry [2], tilted magnetic anisotropy [4,5], exchange bias from the antiferromagnet [8], and interlayer exchange coupling [9].

Another approach for field-free switching is to get assistance from spin-transfer torque (STT) [10–14]. In practice, a magnetic tunnel junction (MTJ) is incorporated into a SOT switching device to read out the magnetic state of the ferromagnetic layer. Therefore, the STT acting on the ferromagnetic layer can also be excited when another electric current is applied to the MTJ. The STT caused by spin current injection from a perpendicularly magnetized reference layer in the MTJ moves the magnetization to an appropriately switched direction and results in deterministic switching. Here, the STT strength, or, equivalently, the current density flowing in the MTJ, should be carefully tuned. If the STT strength is weak, the switching will still be probabilistic. Therefore, understanding the relationship between the STT strength and the switching probability is of great interest.

In this work, we perform numerical simulations of the Landau-Lifshitz-Gilbert (LLG) equation and evaluate the probability of SOT driven magnetization switching, assisted by STT, in a perpendicularly magnetized ferromagnet. In a weak STT region, the switching probability increases monotonically as the STT strength increases, as expected. However, as the STT strength further increases close to a critical value, we observe a decrease in the switching probability, which is contrary to the intuition that STT prompts the switching. The

*tomohiro-taniguchi@aist.go.jp

number of switching errors is on the order of 10–100 among 10^7 trials, which looks small but is non-negligible for practical applications. To clarify the origin of the switching error, we perform a statistical analysis of the magnetization direction in the presence of SOT and STT and solve the LLG equation analytically. We find that there is an inactive region in the Bloch sphere where the SOT becomes less effective for switching due to its cancellation by the precessional torque from the perpendicular magnetic anisotropy field. In this region, the dynamics in the perpendicular direction is determined mainly by the STT and becomes very slow. Since the region of this slow dynamics is located far away from the initial state of the magnetization, a strong STT is required; this is the reason why the number of switching errors increases as the STT strength increase. In addition, assistance from thermal activation is necessary to move the magnetization to this region. As a result, the slow dynamics is induced probabilistically. The results indicate that the STT strength should be carefully tuned for reliable switching. Based on the theoretical analysis of the slow dynamics, we also propose two methods to improve the switching probability; one is to reduce the duration that STT is applied prior to application of SOT, and the other is to enhance the SOT strength.

This paper is organized as follows. In Sec. II A, the system description and the definition of the switching probability are given. The decrease in the switching probability in a large STT region is also shown. In Sec. III, the origin of the switching error is investigated. Proposals to improve the switching error are also presented. Section IV is devoted to the conclusion.

II. THEORETICAL FORMULATION FOR EVALUATING MAGNETIZATION SWITCHING PROBABILITY

Here, we provide a system description and explain the method for evaluating the switching probability.

A. System description

Figure 1(a) shows a schematic illustration of the system under consideration. An MTJ, consisting of a bottom free layer, a nonmagnetic spacer, and a top reference layer, is placed on an electrode. The z axis is perpendicular to the film plane of the MTJ. The unit vectors **m** and **p** ($= +\mathbf{e}_z$) represent the magnetization directions of the free and reference layers in the MTJ. Here, $\mathbf{e}_k$ ($k = x, y, z$) is the unit vector in the k direction. We use the macrospin assumption because such a simplified dynamics is desirable in practice. Studies beyond the macrospin assumption are reported in Refs. [15–18], for example. Electric current flowing in the MTJ excites the STT acting on **m**, where the current density is denoted as j_{STT}. A positive current flowing in the MTJ is defined as the current from the reference to the free layer, i.e. along the $-z$ direction in Fig. 1(a). For positive current, the electrons reflected by the spacer are injected into the free layer and excite STT, which moves the magnetization to the direction antiparallel to **p**, i.e., the $-z$ direction. On the other hand, j_{SOT} represents the current density flowing in the bottom electrode. Positive j_{SOT} indicates current flowing along $+x$ direction. Because of the spin Hall effect [19–22], the electrons carrying j_{SOT} experience spin-dependent scattering and are injected into the free
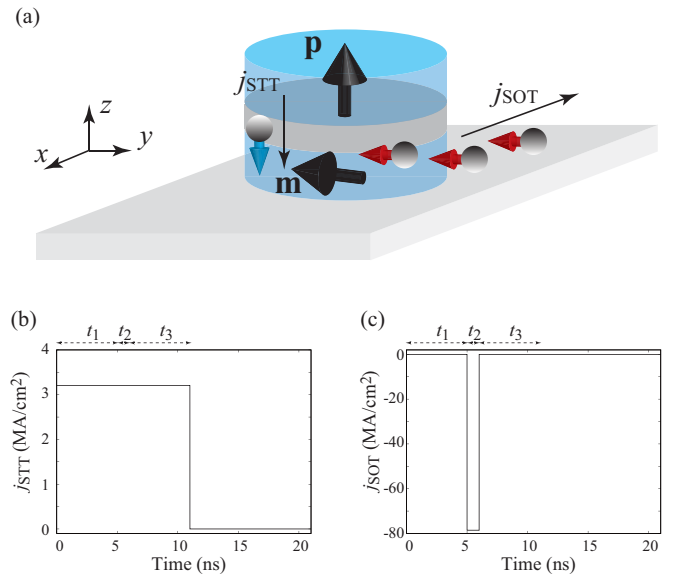

FIG. 1. (a) Schematic illustration of a three-terminal device. The z axis is perpendicular to the film plane of the MTJ. The unit vectors **m** and **p** ($= +\mathbf{e}_z$) represent the magnetization directions of the free and reference layers in the MTJ. The current densities exciting the STT and SOT are denoted as j_{STT} and j_{SOT}, respectively. In the present studies, we assume positive STT and negative SOT currents, which flows in the negative z and x directions, respectively. Note that the directions of the currents are opposite to the moving directions of the electrons. For the positive STT current, the electrons reflected by the spacer and polarized in the negative z direction is injected into the free layer. The time dependence of (b) j_{STT} and (c) j_{SOT}. From $t = 0$ to $t = t_1$, only j_{STT} is applied. At $t = t_1$, j_{SOT} is also applied. At $t = t_1 + t_2$, j_{SOT} is turned off, and j_{STT} is also turned off at $t = t_1 + t_2 + t_3$. In this example, $t_1 = 5$ ns, $t_2 = 1$ ns, and $t_3 = 5$ ns.

layer as pure spin current, which excites SOT. In this work, we assume that the material of the bottom electrode has a negative spin Hall effect, as in the case of tungsten [23–26], and set j_{SOT} to be negative for convenience. Accordingly, the SOT moves the magnetization to the $-y$ direction [see Fig. 1(a) for the definition of the coordinate axis]. The magnetization dynamics driven by the STT and SOT are described by the LLG equation, whose details are given in next section.

B. Landau-Lifshitz-Gilbert equation

Here, we describe the LLG equation. The LLG equation is

$$\frac{d\mathbf{m}}{dt} = -\gamma \mathbf{m} \times \mathbf{H} - \gamma H_{STT}\mathbf{m} \times (\mathbf{p} \times \mathbf{m})$$
$$- \gamma H_{SOT}\mathbf{m} \times (\mathbf{e}_y \times \mathbf{m}) + \alpha \mathbf{m} \times \frac{d\mathbf{m}}{dt}, \quad (1)$$

where the magnetic field $\mathbf{H} = H_K m_z \mathbf{e}_z$ includes only the perpendicular magnetic anisotropy field ($H_K > 0$). The parameters γ and α are the gyromagnetic ratio and the Gilbert damping constant, respectively. The STT strength H_{STT} in units of magnetic field is [27]

$$H_{STT} = \frac{\hbar \eta j_{STT}}{2e(1 + \lambda \mathbf{m} \cdot \mathbf{p})Md}, \quad (2)$$

where η is the spin polarization of the current flowing in the MTJ and λ determines the angular dependence of the STT. The parameters M and d are the saturation magnetization and the thickness of the free layer. On the other hand, the SOT strength is given by

$$H_{\text{SOT}} = \frac{\hbar \vartheta \, j_{\text{SOT}}}{2eMd},$$ (3)

where ϑ is the spin Hall angle.

Since we study STT-assisted SOT switching, it is convenient to introduce critical current densities. The definition of the critical current density is that, when the current density becomes larger than the critical value, the magnetization switches direction at zero temperature. For STT switching, the critical current density is [28,29]

$$j_{\text{c,STT}} = \frac{2e\alpha Md}{\hbar \eta} H_{\text{K}},$$ (4)

when λ is assumed to be small. We introduce the ratio r_{STT} to characterize the STT strength:

$$r_{\text{STT}} = \frac{j_{\text{STT}}}{j_{\text{c,STT}}}.$$ (5)

Since we are interested in STT-assisted SOT switching, we focus on the parameter region with $r_{\text{STT}} \leqslant 1$. On the other hand, the critical current density of SOT switching was formulated in Ref. [30], although a similar formula was derived in Ref. [31] for a different purpose. The formula in the absence of an external magnetic field is

$$j_{\text{c,SOT}} = \frac{eMd}{\hbar \vartheta} H_{\text{K}}.$$ (6)

Like in Eq. (5), we introduce

$$r_{\text{SOT}} = \frac{j_{\text{SOT}}}{j_{\text{c,SOT}}}.$$ (7)

Note that $j_{\text{c,STT}}$ is proportional to the Gilbert damping constant α, which is usually small [32], while $j_{\text{c,SOT}}$ is independent of it. Therefore, the SOT strength is usually larger than the STT. This fact will affect the dependence of the magnetization switching probability on j_{STT}, as discussed below.

C. Current pulse scheme

Here, we describe the scheme of current injection in this work. Although past studies assumed simultaneous injection of j_{STT} and j_{SOT} [14], aligning the beginning of the current pulses so that they start at exactly the same time is experimentally challenging. Since $j_{\text{c,SOT}}$ is large and the SOT induces fast switching [30], it is desirable to make the duration of j_{SOT} short for a low-power writing scheme. Accordingly, in this work, we assume that the current density j_{STT} for the STT is applied from time $t = 0$. Next, the current density j_{SOT} for the SOT is also applied from $t = t_1$ and is turned off at $t = t_2$; that is, j_{SOT} is applied in the range of $t_1 \leqslant t < t_1 + t_2$. After that, j_{STT} is also turned off at $t = t_1 + t_2 + t_3$; that is, j_{STT} is applied in the range of $0 \leqslant t < t_1 + t_2 + t_3$. Figures 1(b) and 1(c) show examples of the time dependence of j_{STT} and j_{SOT}, respectively, where we assume that $j_{\text{STT}} = j_{\text{c,STT}}$ and $j_{\text{SOT}} = j_{\text{c,SOT}}$. The timescales are $t_1 = 5$ ns, $t_2 = 1$ ns, and $t_3 = 5$ ns in this example.

TABLE I. Parameters used in the numerical calculations: M, saturation magnetization; H_{K}, perpendicular magnetic anisotropy field; γ, gyromagnetic ratio; α, Gilbert damping constant; d, thickness of the free layer; V, volume of the free layer; η, spin polarization ($\lambda = \eta^2$); ϑ, spin Hall angle of the tungsten electrode.

Quantity	Value
M	$1500 \, \text{emu/cm}^3$
H_{K}	$1.172 \, \text{kOe}$
γ	$1.764 \times 10^7 \, \text{rad/(Oe s)}$
α	0.030
d	$1 \, \text{nm}$
V	$d \times \pi \times 30^2 \, \text{nm}^3$
η	0.5
ϑ	-0.34

D. Definition of switching probability

We add a random torque $-\gamma \mathbf{m} \times \mathbf{h}$ to the right-hand side of Eq. (1) to describe the thermally activated magnetization dynamics. Component h_k ($k = x, y, z$) of the random field $\mathbf{h}$ satisfies the fluctuation-dissipation theorem [33],

$$\langle h_k(t) h_\ell(t') \rangle = \frac{2\alpha k_{\text{B}} T}{\gamma MV} \delta(t - t'),$$ (8)

where T and V are the temperature and volume of the free layer. A numerical method to solve Eq. (1) using Eq. (8) was described in our previous work [34].

In the present study, we solve the LLG equation without STT and SOT for 10 ns with the condition $\mathbf{m}(t = -10 \, \text{ns}) = +\mathbf{e}_z$. Then, the magnetization direction at $t = 0$ ns is randomly distributed around the z axis. After that, we solve the LLG equation with current from $t = 0$ to $t = t_1 + t_2 + t_3$ by using the current pulse scheme described in Sec. II C. After $t = t_1 + t_2 + t_3$, we solve the LLG equation without STT and SOT for 10 ns again. The magnetization switching is studied to determine whether $m_z < 0$ or not at this moment. We repeat this process 10^7 times and evaluate the switching probability. The values of the parameters are summarized in Table I [26], where the value of H_{K} is set such that the thermal stability $\Delta_0 = MH_{\text{K}}V/(2k_{\text{B}}T)$ at room temperature ($T = 300$ K) equals to 60. Using these values, the critical current densities of STT and SOT switching, $j_{\text{c,STT}}$ and $j_{\text{c,SOT}}$, are estimated to be 3.2 and $-78.6 \, \text{MA/cm}^2$, respectively.

Figure 2(a) shows an example of the magnetization dynamics driven by STT and SOT, where $r_{\text{STT}} = 1.0$ and $r_{\text{SOT}} = 1.0$ while $t_1 = 5$ ns, $t_2 = 1$ ns, and $t_3 = 5$ ns. From $t = 0$ to $t = t_1$, only the STT acts on the magnetization. The STT compensates the damping torque, and thus, the deviation of the magnetization from the z axis is tiny. When j_{SOT} is applied from $t = t_1$, the magnetization immediately moves to the negative y direction due to the SOT. At $t = t_1 + t_2$, the magnetization slightly shifts toward $-\mathbf{e}_z$ because of the STT pointing in the negative z direction. After j_{SOT} is turned off, the magnetization nearly reaches the switched state ($\mathbf{m} = -\mathbf{e}_z$). At $t = 21$ ns, $m_z \simeq -1$, and thus, this trial is regarded as a successful case of the magnetization switching. Figure 2(b) summarizes the dependence of the switching probability on $r_{\text{STT}} = j_{\text{STT}}/j_{\text{c,STT}}$. When $r_{\text{STT}} = 0$, the
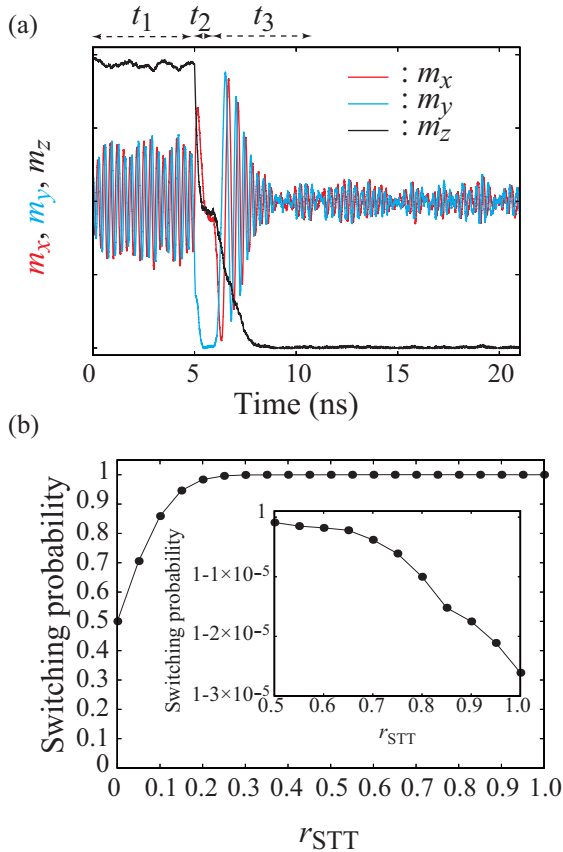
FIG. 2. (a) An example of time evolution of m_x (red), m_y (blue), and m_z (black). Times are $t_1 = 5$ ns, $t_2 = 1$ ns, and $t_3 = 5$ ns in this example, while currents are $j_{\text{STT}} = j_{c,\text{STT}}$ ($r_{\text{STT}} = 1.0$) and $j_{\text{SOT}} = j_{c,\text{SOT}}$ ($r_{\text{SOT}} = 1.0$). (b) Dependence of the magnetization switching probability on $r_{\text{STT}} = j_{\text{STT}}/j_{c,\text{STT}}$. The inset is an enlarged view of the probability for $r_{\text{STT}} \geqslant 0.5$, where the range of the vertical axis is from $1 - 3 \times 10^{-5}$ to 1.

switching probability is approximately 0.5. The switching probability increases as the STT (r_{STT}) increases and reaches 1.0 when $r_{\text{STT}} = 0.5$. This is reasonable because the STT points in the $-z$ direction.

However, we find that the switching probability slightly decreases with increasing r_{STT}, as indicated in the inset in Fig. 2(b). The result is contrary to intuition, in which the switching probability monotonically increases as the STT increases. Recall that we performed the LLG simulation 10^7 times for each r_{SOT}. Therefore, the result indicates that trials on the order of 10–100 fail to switch the magnetization for relatively large r_{STT} (> 0.5). Although the decrease in the probability is small, it is non-negligible for practical purposes such as magnetoresistive random-access memory. For example, an error rate less than 10^{-3} for storage memory or 10^{-9} for working memory is required [35–37]. In the next section, we investigate the physical origin of this unexpected decrease in the switching probability and propose methods to reduce the switching errors.

Although the macrospin model used here can capture the essential features of magnetization switching processes, micromagnetic simulations are preferred to assess the error rate of a more realistic device. For example, domain nucleation

and subsequent domain wall propagation may play a role in defining the switching probability. Further studies are required to understand how such micromagnetic processes influence the error rate in memory devices.

III. THEORETICAL ANALYSIS OF THE SWITCHING ERROR

In this section, we investigate the origin of the failure of the magnetization switching. Based on the analysis, we also study methods to decrease the switching error.

A. Histogram of magnetization direction

We notice that a statistical analysis of the magnetization direction through an evaluation of histogram for $\theta = \cos^{-1} m_z$ provides a hint of the origin of the switching error. Figures 3(a), 3(b), and 3(c) are histograms at $t = t_1$, $t = t_1 + t_2$, and $t = t_1 + t_2 + t_3$, respectively. The blue and red circles correspond to $r_{\text{STT}} = 0.5$ and 1.0, respectively. When $j_{\text{SOT}} = 0$, the magnetization mainly stays near the initial state ($m_z \simeq +1$), as shown in Fig. 3(a). For a large STT, however, there are some trials where the magnetization switches direction ($m_z < 0$) even in the absence of SOT. These results are reasonable because the STT moves the magnetization to the negative z direction; however, since $r_{\text{SOT}} \leqslant 1.0$, the magnetization mainly remains near the initial state.

An unexpected behavior appears when j_{SOT} is applied and r_{STT} is relatively large, as shown in Fig. 3(b). Recall that the SOT moves the magnetization to the $-y$ direction, where $m_z = 0$ (or, equivalently, $\theta = 90°$). Note also that the magnitude of the SOT is significantly larger than that of the STT because $j_{c,\text{SOT}}/j_{c,\text{STT}} = 1/(2\alpha) \gg 1$. Therefore, the histogram was expected to have a peak near $\theta = 90°$ but slightly shifted in the switching direction ($\theta = 180°$) due to the STT. The histogram for weak STT ($r_{\text{STT}} = 0.5$) matches this expectation, as shown in Fig. 3(b). However, the histogram for strong STT ($r_{\text{STT}} = 1.0$) shows an asymmetric distribution and represents several trials near $30° \leqslant \theta \ll 90°$. Such an asymmetric, small distribution in the region of $\theta \ll 90°$ appears for $r_{\text{STT}} \gtrsim 0.70$. We emphasize that this small distribution is in contrast to our intuition because the STT moves the magnetization to the negative z direction, and the STT strength is close to the critical value. We confirmed that some trials in this small distribution cannot reach the switched region ($\theta > 90°$) even after j_{STT} is turned off and, consequently, are failed trials [see Fig. 3(c)].

Based on the results, we investigate the origin of the small distribution appearing in the region of $\theta < 90°$, as shown by the red circles in Fig. 3(b), where both STT and SOT are excited.

B. Origin of switching error

Figures 4(a)–4(c) show 10 examples of m_x, m_y, and m_z when the magnetization switching is successful. The time range is from $t = 0$ to $t = t_1 + t_2 + t_3$, while $r_{\text{STT}} = j_{\text{STT}}/j_{c,\text{STT}} = 1.0$ and $r_{\text{SOT}} = j_{\text{SOT}}/j_{c,\text{SOT}} = 1.0$. Like in Fig. 2(a), m_z remains close to the initial state ($m_z \simeq +1$) even after j_{STT} is turned on ($t \leqslant t_1$). When j_{SOT} is turned on at $t = t_1$, the magnetization immediately moves to the negative
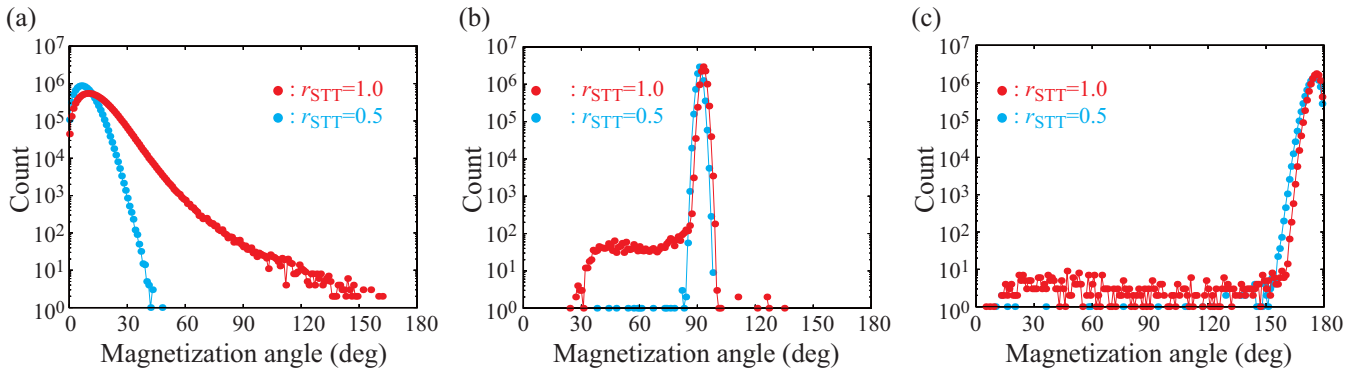
FIG. 3. Histograms of the magnetization angle ($\theta = \cos^{-1} m_z$) from the z axis just before (a) j_{SOT} is turned on ($t = t_1$), (b) j_{SOT} is turned off ($t = t_1 + t_2$), and (c) j_{STT} is turned off ($t = t_1 + t_2 + t_3$). The current density for the STT j_{STT} is $r_{\mathrm{STT}} = j_{\mathrm{STT}}/j_{\mathrm{c,STT}} = 0.5$ for blue circles and $r_{\mathrm{STT}} = 1.0$ for red circles. Times are $t_1 = 5$ ns, $t_2 = 1$ ns, and $t_3 = 5$ ns. The current density for the SOT is $j_{\mathrm{SOT}} = j_{\mathrm{c,SOT}}$ ($r_{\mathrm{SOT}} = 1.0$).

y direction with a slight shift in the negative z direction. After j_{SOT} is turned off at $t = t_1 + t_2$, the magnetization moves to the negative z direction due to the STT. Since we are interested in the magnetization direction in the presence of both STT and SOT, as mentioned above, we also show enlarged views of m_x, m_y, and m_z to $t = t_1 + t_2$ in Figs. 4(d)–4(f). Here, we can confirm that m_z remains near $m_z \geqslant 0.9$.

Ten examples of m_x, m_y, and m_z for failed trials are shown in Figs. 5(a)–5(c). Enlarged views to $t = t_1 + t_2$ are shown in Figs. 5(d)–5(f). Comparing them with Fig. 4, we notice

the following two points. First, when the switching fails, the dynamics of m_x and m_y approximately stop at points with $m_x > 0$ and $m_y \simeq 0$ when j_{SOT} is turned on at $t = t_1$. This is in contrast to the successful case in Fig. 4, where m_y immediately moves to -1. Second, m_z just before the SOT is turned on is relatively small; that is, the magnetization largely tilts from the z axis, which can be seen from a comparison of Figs. 4(f) and 5(f).

We find that these differences in the dynamics of the successful and failed samples can be explained as follows. It is
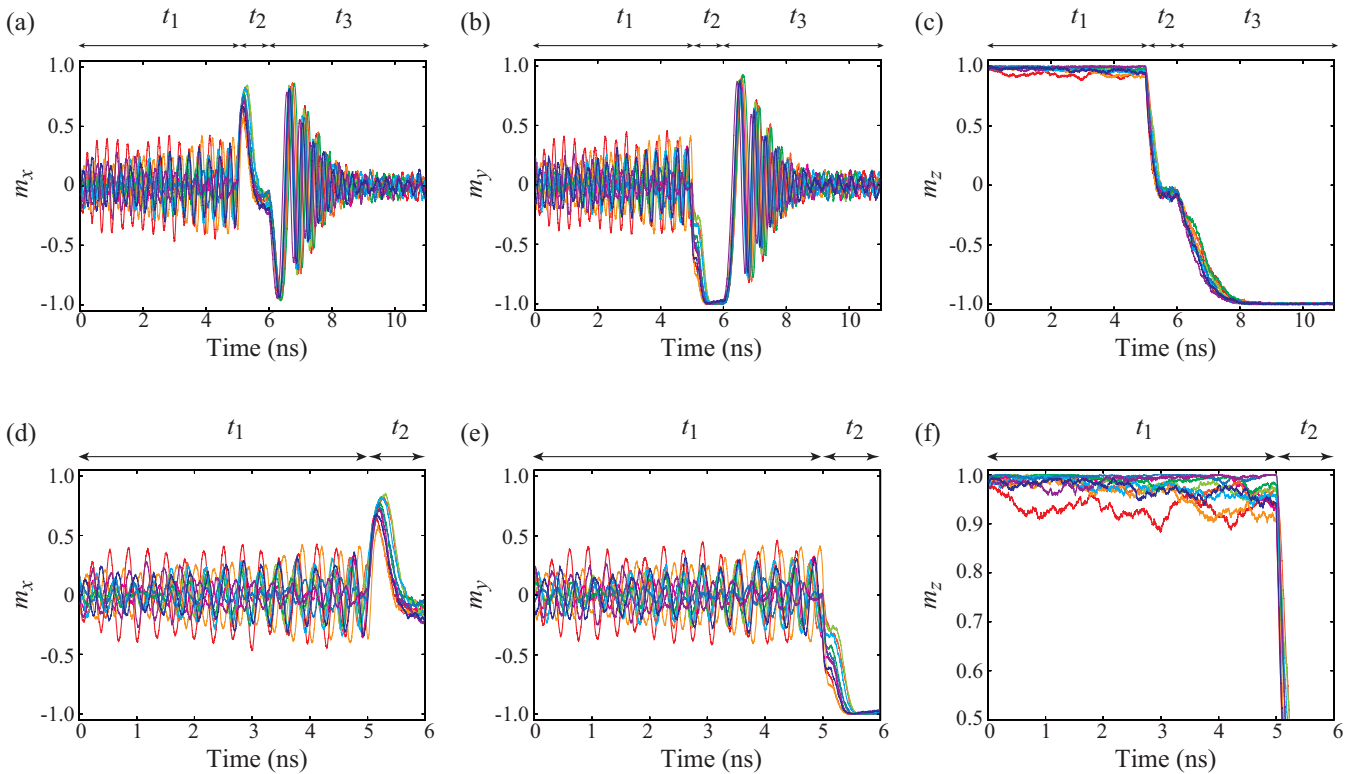

FIG. 4. Time evolution of (a) m_x, (b) m_y, and (c) m_z for 10 successful samples of magnetization switching. The time range is from $t = 0$ to $t = t_1 + t_2 + t_3$. Note that j_{STT} is turned on at $t = 0$, j_{SOT} is turned on at $t = t_1$, j_{SOT} is turned off at $t = t_1 + t_2$, and j_{STT} is turned off at $t = t_1 + t_2 + t_3$. The current densities are $j_{\mathrm{STT}} = j_{\mathrm{c,STT}}$ ($r_{\mathrm{STT}} = 1.0$) and $j_{\mathrm{SOT}} = j_{\mathrm{c,SOT}}$ ($r_{\mathrm{SOT}} = 1.0$). (d)–(f) Enlarged views from $t = 0$ to $t = t_1 + t_2$.
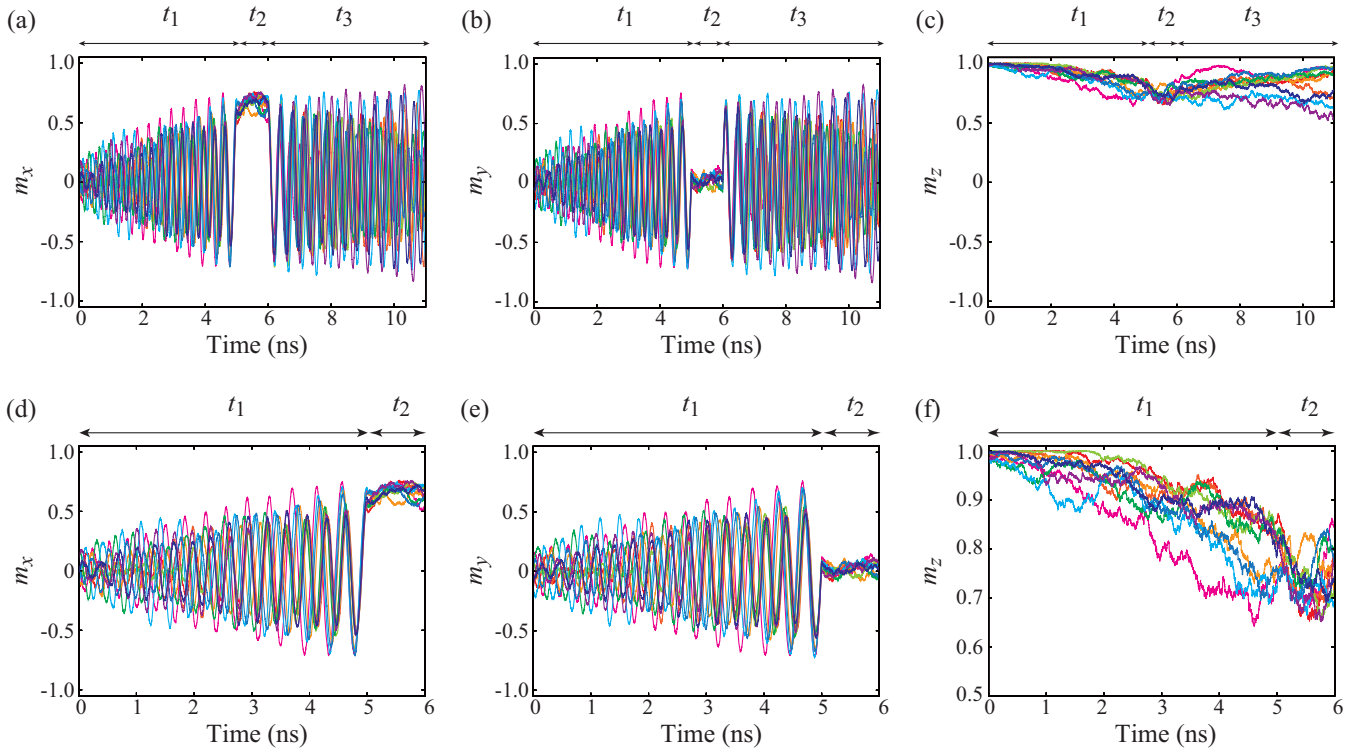
FIG. 5. Time evolution of (a) m_x, (b) m_y, and (c) m_z for 10 failed samples of magnetization switching. The time range is from $t = 0$ to $t = t_1 + t_2 + t_3$. Note that j_{STT} is turned on at $t = 0$, j_{SOT} is turned on at $t = t_1$, j_{SOT} is turned off at $t = t_1 + t_2$, and j_{STT} is turned off at $t = t_1 + t_2 + t_3$. The current densities are $j_{\mathrm{STT}} = j_{\mathrm{c,STT}}$ ($r_{\mathrm{STT}} = 1.0$) and $j_{\mathrm{SOT}} = j_{\mathrm{c,SOT}}$ ($r_{\mathrm{SOT}} = 1.0$). (d)–(f) Enlarged views from $t = 0$ to $t = t_1 + t_2$.

convenient for the explanation to express Eq. (1) in terms of $\theta = \cos^{-1} m_z$ and $\varphi = \tan^{-1}(m_y/m_x)$, which correspond to the tilted angle from the z axis and the phase in the xy plane:

$$\frac{1 + \alpha^2}{\gamma} \frac{d\theta}{dt} = H_{\mathrm{STT}} \sin\theta - H_{\mathrm{SOT}} \cos\theta \sin\varphi - \alpha H_{\mathrm{K}} \sin\theta \cos\theta + \alpha H_{\mathrm{SOT}} \cos\varphi, \tag{9}$$

$$\frac{1 + \alpha^2}{\gamma} \sin\theta \frac{d\varphi}{dt} = H_{\mathrm{K}} \sin\theta \cos\theta - H_{\mathrm{SOT}} \cos\varphi + \alpha H_{\mathrm{STT}} \sin\theta - \alpha H_{\mathrm{SOT}} \cos\theta \sin\varphi. \tag{10}$$

Here, the random torque due to thermal activation is neglected for simplicity. Also, we use the approximation $1 + \alpha^2 \simeq 1$ for simplicity.

Let us first consider the successful case. As implied by Fig. 4(f), θ just before the injection of j_{SOT} is close to the initial state ($\theta \simeq 0°$). The SOT moves the magnetization to the $-y$ direction for the present definitions of the signs of ϑ and j_{SOT}. Equation (9) dictates that θ near the initial state obeys $d\theta/dt \simeq \gamma H_{\mathrm{SOT}}$, where we neglect terms proportional to the small constant α. In addition, recall that H_{STT} is also on the order of αH_{K} because $j_{\mathrm{STT}} \leqslant j_{\mathrm{c,STT}} \propto \alpha H_{\mathrm{K}}$. Note that $1/(\gamma H_{\mathrm{SOT}})$ is on the order of 0.1 ns, which indicates that the magnetization moves from the z to the y direction immediately, as schematically shown in Fig. 6(a). This is consistent with the result shown in Fig. 4(e).

For the failed trial, we should recall that θ just before the injection of j_{SOT} is relatively large. This happens when the random torque due to thermal activation coincidentally

assists the STT continuously and moves the magnetization away from the z axis. We should also recall that, after j_{SOT} is turned on, m_x and m_y approximately stop their dynamics at $m_x > 0$ and $m_y \simeq 0$ for the failed trials. In fact, we notice that Eq. (10) has a solution of $d\varphi/dt \simeq 0$ when $\varphi \simeq 0$ and $\theta \simeq \theta_c$, where a critical angle θ_c satisfies

$$\sin 2\theta_c \simeq \frac{2H_{\mathrm{SOT}}}{H_{\mathrm{K}}} = r_{\mathrm{SOT}}, \tag{11}$$

where we used Eqs. (3), (6), and (7). Recall that we are interested in the switching mainly driven by SOT, and thus, $r_{\mathrm{SOT}} = j_{\mathrm{SOT}}/j_{\mathrm{c,SOT}}$ should satisfy $r_{\mathrm{SOT}} \geqslant 1$. Therefore, θ_c is finite only when $r_{\mathrm{SOT}} \simeq 1$ and thus θ_c is close to $45°$. One might consider that only $r_{\mathrm{SOT}} = 1$ is a possible solution of Eq. (11) to make θ_c a real number. We should, however, remember that some assumptions and approximations, such as $\varphi \simeq 0°$ when $d\varphi/dt \simeq 0$ and $\alpha H_{\mathrm{STT}} \ll H_{\mathrm{SOT}}$, are used in the derivation of Eq. (11); therefore, we consider the fixed
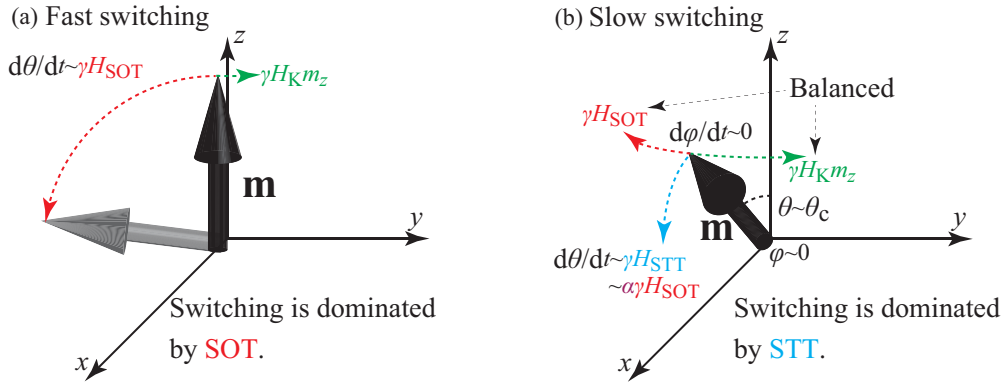
FIG. 6. Schematic illustrations of dominant torques for (a) successful and (b) failed trials of magnetization switching. (a) When the magnetization is stabilized near the z direction, the SOT dominantly moves the magnetization from the z axis. The time evolution of $\theta = \cos^{-1} m_z$ is roughly described as $d\theta/dt \simeq \gamma H_{\mathrm{SOT}}$. (b) If the magnetization locates in the xz plane with $m_x > 0$ [i.e., $\varphi = \tan^{-1}(m_y/m_x) = 0$] and θ is close to a critical value θ_c when j_{SOT} is turned on, the SOT completely points in the y direction and balances the precessional torque due to magnetic field ($\propto \gamma H_K m_z$), i.e., $d\varphi/dt \sim 0$. In this case, the SOT does not contribute to $d\theta/dt$, and $d\theta/dt$ is mainly determined by the STT. Since the STT ($\propto \gamma H_{\mathrm{STT}}$) is on the order of $\alpha \gamma H_K(\sim \alpha \gamma H_{\mathrm{SOT}})$, $d\theta/dt$ is relatively slow.

point of φ, satisfying $d\varphi/dt \simeq 0$, to appear near $r_{\mathrm{SOT}} \simeq 1$, but this equation is not restricted strictly to $r_{\mathrm{SOT}} = 1$. In fact, m_z of the failed samples in Fig. 5(f) are close to $\cos 45° \simeq 0.7$ when j_{SOT} is applied at $t = t_1$. If we substitute $\varphi \simeq 0°$ and $\theta \simeq \theta_c \simeq 45°$, Eq. (9) gives

$$\frac{1}{\gamma}\frac{d\theta}{dt} \simeq \frac{\alpha H_K}{2}(\sqrt{2}r_{\mathrm{STT}} - 1 + r_{\mathrm{SOT}}), \tag{12}$$

where we use Eqs. (2)–(7). Note that θ in this case changes slowly because the right-hand side of Eq. (12) is proportional to the small constant α. Because $r_{\mathrm{SOT}} \simeq 1$ is of interest here, Eq. (12) might be further approximated as $d\theta/dt \simeq \gamma \alpha H_K r_{\mathrm{STT}}/\sqrt{2}$. This is in contrast to the successful case mentioned above, in which $d\theta/dt \sim \gamma H_{\mathrm{SOT}}$ is independent of α. Because of the presence of α in Eq. (12), the magnetization in some trials changes direction slowly and cannot reach the y direction even in the presence of the SOT. This leads to the distribution in the region of $\theta \ll 90°$ shown in Fig. 3(b). The physical interpretation of the above results is as follows. Recall that the SOT moves the magnetization to the $-y$ direction. The magnetization dynamics driven by this SOT often accompanies the change in m_z, as schematically shown in Fig. 6(a). However, if the magnetization coincidentally locates on the line with $m_y = 0$, the SOT exactly points in the y direction and thus does not change m_z. Even if this happens, it usually does not matter because the SOT and/or the precessional torque from the perpendicular magnetic anisotropy field immediately shift the magnetization from this line. Then, the SOT has a projection in the z direction and changes m_z immediately. Therefore, the SOT works effectively to move the magnetization from the z axis.

However, there is an exceptional region on this line ($m_y = 0$), where $\theta \simeq \theta_c$ and $m_x > 0$ [see also Fig. 6(b)]. In this region, the SOT ($\propto \gamma H_{\mathrm{SOT}}$) pointing in the $-y$ direction balances the precessional torque from the perpendicular magnetic anisotropy field ($\propto \gamma H_K m_z$) pointing in the $+y$ direction. Thus, the magnetization direction in the xy plane is fixed, which means that $d\varphi/dt \simeq 0$ at $\varphi \simeq 0°$. This corresponds to the results shown in Figs. 5(d) and 5(e), where m_x and m_y

in $t_1 \leqslant t < t_1 + t_2$ are almost fixed. In this case, the magnetization cannot shift from the line of $m_y = 0$, and therefore, the SOT does not change m_z directly. The dynamics of m_z is driven by the STT, the damping torque reducing the perpendicular magnetic anisotropy energy, and the term proportional to αH_{SOT} in Eq. (9). In particular, the last two terms approximately cancel each other out, as mentioned below Eq. (12). Therefore, the dynamics of m_z is mainly determined by the STT, which is on the order of αH_K and thus is weak. Accordingly, m_z changes slowly and cannot reach, for example, $m_z = 0$, in contrast to the successful case.

In summary, there is an inactive region of the SOT-driven magnetization switching where the magnetization cannot move in the xy plane because of the balance between the SOT and the precessional torque. If the magnetization locates in this region, the SOT is less effective for switching. In this region, the order of the torque moving the magnetization from the z axis is proportional to the damping constant α and thus is small. Therefore, the magnetization cannot reach the point $\theta = 90°$ and has a distribution in the region with $\theta \ll 90°$, as shown in Fig. 3(b). In some of these trials switching fails after both STT and SOT are turned off.

These considerations also explain why the magnetization switching probability decreases as j_{STT} ($\propto r_{\mathrm{STT}}$) increases, as shown in the inset in Fig. 2(b). As mentioned, the slow change in θ, or, equivalently m_z, occurs when θ, m_x, and m_y simultaneously satisfy $\theta \simeq \theta_c$, $m_x > 0$, and $m_y \simeq 0$. Note that the condition $\theta \simeq \theta_c$ is satisfied when the STT is relatively large because $\theta_c \simeq 45°$ greatly deviates from the initial state ($\theta \simeq 0°$). In other words, a large STT is required to satisfy the conditions of the switching error. Therefore, the magnetization switching probability shows a decrease in a relatively large r_{STT} region. Simultaneously, we emphasize that it is rare to satisfy these three conditions simultaneously, even in the presence of random torque. In addition, even if these conditions are satisfied and the magnetization dynamics becomes slow when the SOT exists, the STT after the SOT is turned off usually moves the magnetization to the switched direction. Therefore, the decrease in the magnetization switching
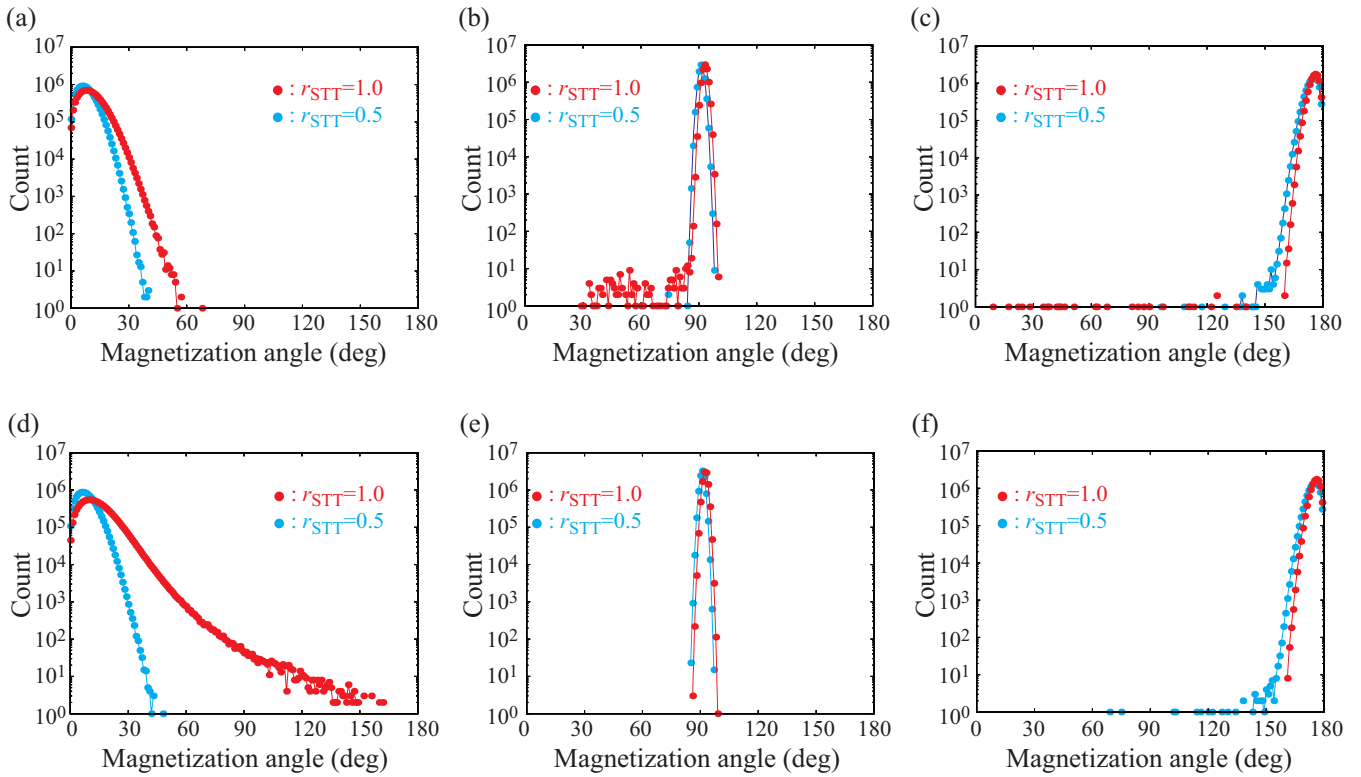
FIG. 7. Histograms of the magnetization angle ($\theta = \cos^{-1} m_z$) from the z axis just before (a) j_{SOT} is turned on ($t = t_1$), (b) j_{SOT} is turned off ($t = t_1 + t_2$), and (c) j_{STT} is turned off ($t = t_1 + t_2 + t_3$). The current density for the STT j_{STT} is $r_{STT} = j_{STT}/j_{c,STT} = 0.5$ for blue circles and $r_{STT} = 1.0$ for red circles. Times t_1 is 2 ns in this example, while $t_2 = 1$ ns, $t_3 = 5$ ns, and $j_{SOT} = j_{c,SOT}$ ($r_{SOT} = 1.0$) are the same as in Fig. 3. (d)–(f) Histograms for $t_1 = 5$ ns and $j_{SOT} = 1.2 j_{c,SOT}$ ($r_{SOT} = 1.2$).

probability is relatively small; however, the switching errors cannot be neglected for practical purpose.

As mentioned below Eqs. (11) and (12), approximations were used in the derivation of θ_c. Thus, even if θ at $t = t_1$ is not exactly identical to θ_c, switching may fail. In addition, the random torque plays a role in moving the magnetization to a point satisfying the conditions $\theta \simeq \theta_c$, $m_x > 0$, and $m_y \simeq 0$. Thus, the failure is even probabilistic. There will be a range of θ for failed switching; however, its specification is difficult and is beyond the scope of this paper.

The conditions $\theta_c \simeq 45°$ and $\varphi \simeq 0°$ for the slow dynamics of θ arise from the fact that ϑj_{SOT} in the present work is positive and the magnetization initially points in the positive z direction. When ϑj_{SOT} is negative or the initial state is close to the negative z direction, the balance between the SOT and the precessional torque occurs at $\varphi \simeq 180°$ or $\theta_c \simeq 135°$. Therefore, the slow dynamics is unavoidable even if the material, the sign of the current, or the initial direction is changed.

C. Improvement of the switching error

The analyses in Sec. III B imply methods for improving the switching error and keeping the switching probability high even in a strong STT region. The point is to avoid events where the magnetization arrives at the point $\theta \simeq \theta_c$ and $\varphi \simeq 0°$.

The first proposal is to reduce the time t_1. Recall that only j_{STT} is injected from $t = 0$ and $t = t_1$, and the slow dynamics

occurs when θ at $t = t_1$ is close to θ_c. Since θ_c is far from the initial direction ($\theta \simeq 0°$), θ at $t = t_1$ will not reach θ_c if t_1 is short. Based on this idea, we perform a numerical simulation in which t_1 is shortened to 2 ns. Figures 7(a)–7(c) show the histograms of θ at $t = t_1$, $t = t_1 + t_2$, and $t = t_1 + t_2 + t_3$, respectively, where j_{SOT} is $r_{SOT} = 1.0$, as in the case in Fig. 3. Let us compare them with those in Fig. 3, in particular for the case of $r_{STT} = 1.0$ shown by the red circles. Comparing Fig. 7(a) with Fig. 3(a), we notice that the number of samples in which θ gets close to θ_c is greatly reduced. Although Fig. 7(b) indicates that there is still a small distribution in the region of $\theta \ll 90°$ at $t = t_1 + t_2$, it is relatively small compared with that in Fig. 3(b). Accordingly, the final distribution after both j_{STT} and j_{SOT} are turned off mostly concentrated near the switched state, as shown in Fig. 7(c).

Another proposal is to inject a relatively large j_{SOT}. According to Eq. (11), θ_c is a real number only when $r_{SOT} \lesssim 1$. This means that the balance between the SOT and the precessional torque occurs only when $r_{SOT} \lesssim 1$. Therefore, the slow dynamics will be avoided when j_{SOT} is sufficiently larger than the critical value $j_{c,SOT}$, although it is not preferable from the viewpoint of a low-power writing method. Figures 7(d)–7(f) show histograms where $r_{SOT} = 1.2$. The time t_1 is 5 ns, as in the case in Fig. 3. In this case, the histograms at $t = t_1$ [Figs. 3(a) and 7(d)] are the same, but the histograms at $t = t_1 + t_2$ are very different [see Figs. 3(b) and 7(e)]. There is no small distribution in the region of $\theta \ll 90°$ in Fig. 7(e). As a result, almost all samples succeed in switching, as shown in Fig. 7(f).
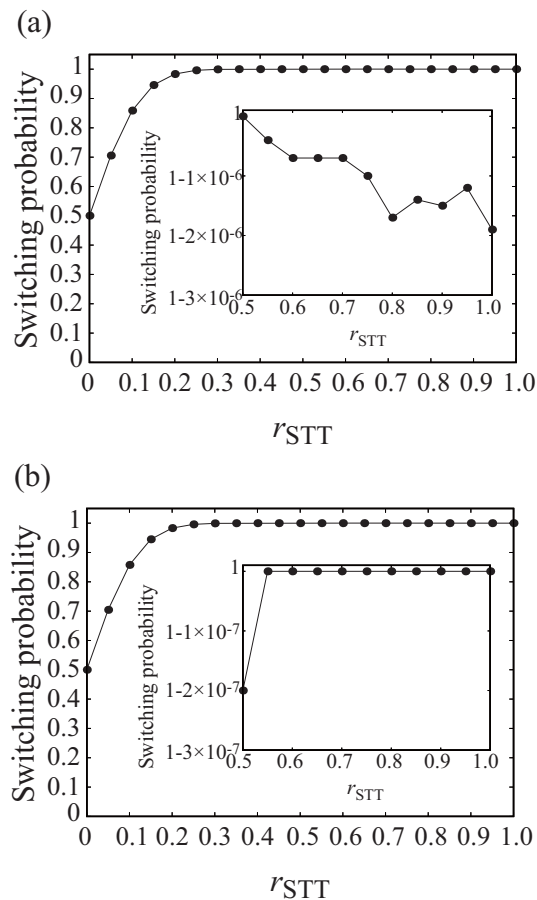
FIG. 8. Dependence of the magnetization switching probability on r_{STT} for (a) $t_1 = 2$ ns and $r_{SOT} = 1.0$ and (b) $t_1 = 5$ ns and $r_{SOT} = 1.2$. The insets are enlarged views for $r_{STT} \geqslant 0.5$. The ranges of the vertical axes of the insets are from $1 - 3 \times 10^{-6}$ to 1 in (a) and from $1 - 3 \times 10^{-7}$ to 1 in (b).

Figure 8 shows the switching probabilities for $t_1 = 2$ ns and $r_{SOT} = 1.0$ [Fig. 8(a)] and $t_1 = 5$ ns and $r_{SOT} = 1.2$ [Fig. 8(b)]. The inset in Fig. 8(a) indicates that there are still errors in the switching, which can be also confirmed from

Fig. 7(c). However, the number of switching error is reduced by one order of magnitude in comparison to the result shown in Fig. 2(b). In the case of using a strong SOT, the error is almost zero among 10^7 trials for a wide range of STT, as can be seen in the inset in Fig. 8(b).

IV. CONCLUSION

In conclusion, the probability of SOT-driven magnetization switching, assisted by STT, was studied by solving the LLG equation at finite temperature numerically. In a weak STT region, the switching probability monotonically increases as the STT strength increases because the STT points in the switched direction. However, a decrease in the switching probability was observed when the STT current was further increased close to the critical current. The number of switching errors was on the order of 10–100 among 10^7 samples, which is non-negligible for practical purposes. The analysis of the LLG equation revealed that the switching error was caused by the presence of an inactive region in the Bloch sphere where the magnetization dynamics became very slow compared with the conventional SOT switching. In this region, the SOT balances the precessional torque due to the perpendicular magnetic anisotropy field and becomes less effective for switching. In this case, the switching is induced by the STT, which is weak for the present switching scheme. Therefore, the dynamics becomes slow, and the magnetization cannot reach the switched state. Since a relatively large STT is required to move the magnetization to this region, the number of switching error increases as the STT strength increases. This is the origin of the unexpected increase in the error rate. Since assistance from thermal activation is also necessary for the magnetization to arrive in the region, the switching error appears probabilistically. The issue can be solved if the time when only the STT is applied is reduced and/or the SOT strength is enhanced.

[1] L. Liu, O. J. Lee, T. J. Gudmundsen, D. C. Ralph, and R. A. Buhrman, Current-induced switching of perpendicularly magnetized magnetic layers using spin torque from the spin Hall effect, Phys. Rev. Lett. **109**, 096602 (2012).

[2] G. Yu, P. Upadhyaya, Y. Fan, J. G. Alzate, W. Jiang, K. L. Wong, S. Takei, S. A. Bender, L.-T. Chang, Y. Jiang, M. Lang, J. Tang, Y. Wang, Y. Tserkovnyak, P. K. Amiri, and K. L. Wang, Switching of a perpendicular magnetization by spin-orbit torques in the absence of external magnetic fields, Nat. Nanotechnol. **9**, 548 (2014).

[3] M. Cubukcu, O. Boulle, M. Drouard, K. Garello, C. O. Avci, I. M. Miron, J. Langer, B. Ocker, P. Gambardella, and G. Gaudin, Spin-orbit torque magnetization switching of a three-terminal perpendicular magnetic tunnel junction, Appl. Phys. Lett. **104**, 042406 (2014).

[4] L. You, O. Lee, D. Bhowmik, D. Labanowski, J. Hong, J. Bokor, and S. Salahuddin, Switching of perpendicularly polarized nanomagnets with spin orbit torque without an external magnetic field by engineering a tilted anisotropy, Proc. Natl. Acad. Sci. USA **112**, 10310 (2015).

[5] J. Torrejon, F. Garcia-Sanchez, T. Taniguchi, J. Sinha, S. Mitani, J.-V. Kim, and M. Hayashi, Current-driven asymmetric magnetization switching in perpendicularly magnetized CoFeB/MgO heterostructures, Phys. Rev. B **91**, 214434 (2015).

[6] A. van den Brink, G. Vermijs, A. Solignac, J. Koo, J. T. Kohlhepp, H. J. M. Swagten, and B. Koopmans, Field-free magnetization reversal by spin-Hall effect and exchange bias, Nat. Commun. **7**, 10854 (2016).

[7] Y.-W. Oh, S. H. C. Baek, Y. M. Kim, H. Y. Lee, K.-D. Lee, C.-G. Yang, E.-S. Park, K.-S. Lee, K.-W. Kim, G. Go, J.-R. Jeong,

B.-C. Min, H.-W. Lee, K.-J. Lee, and B.-G. Park, Field-free switching of perpendicular magnetization through spin-orbit torque in antiferromagnet/ferromagnet/oxide structures, Nat. Nanotechnol. **11**, 878 (2016).

[8] S. Fukami, T. Anekawa, C. Zhang, and H. Ohno, Magnetization switching by spin-orbit torque in an antiferromagnet-ferromagnet bilayer system, Nat. Mater. **15**, 535 (2016).

[9] Y.-C. Lau, D. Betto, K. Rode, J. M. D. Coey, and P. Stamenov, Spin-orbit torque switching without an external field using interlayer exchange coupling, Nat. Nanotechnol. **11**, 758 (2016).

[10] M. Wang, W. Cai, D. Zhu, Z. Wang, J. Kan, Z. Zhao, K. Cao, Z. Wang, Y. Zhang, T. Zhang, C. Park, J.-P. Wang, A. Fert, and W. Zhao, Field-free switching of a perpendicular magnetic tunnel junction through the interplay of spin-orbit and spin-transfer torques, Nat. Electron. **1**, 582 (2018).

[11] E. Grimaldi, V. Krizakova, G. Sala, F. Yasin, S. Couet, G. S. Kar, K. Garello, and P. Gambardella, Single-shot dynamics of spin-orbit torque and spin transfer torque switching in three-terminal magnetic tunnel junctions, Nat. Nanotechnol. **15**, 111 (2020).

[12] S. Pathak, C. Youm, and J. Hong, Impact of spin-orbit torque on spin-transfer torque switching in magnetic tunnel junctions, Sci. Rep. **10**, 2799 (2020).

[13] C. Zhang, Y. Takeuchi, S. Fukami, and H. Ohno, Field-free and sub-ns magnetization switching of magnetic tunnel junctions by combining spin-transfer torque and spin-orbit torque, Appl. Phys. Lett. **118**, 092406 (2021).

[14] D. H. Kang and M. Shin, Critical switching current density of magnetic tunnel junction with shape perpendicular magnetic anisotropy through the combination of spin-transfer and spin-orbit torques, Sci. Rep. **11**, 22842 (2021).

[15] J. Z. Sun, R. P. Robertazzi, J. Nowak, P. L. Trouilloud, G. Hu, D. W. Abraham, M. C. Gaidis, S. L. Brown, E. J. O'Sullivan, W. J. Gallagher, and D. C. Worledge, Effect of subvolume excitation and spin-torque efficiency on magnetic switching, Phys. Rev. B **84**, 064413 (2011).

[16] J. Z. Sun *et al.*, Spin-torque switching efficiency in CoFeB-MgO based tunnel junctions, Phys. Rev. B **88**, 104426 (2013).

[17] G. D. Chaves-O'Flynn, G. Wolf, J. Z. Sun, and A. D. Kent, Thermal stability of magnetic states in circular thin-film nanomagnets with large perpendicular magnetic anisotropy, Phys. Rev. Appl. **4**, 024010 (2015).

[18] J. Z. Sun, Spin-transfer torque switching probability of CoFeB/MgO/CoFeB magnetic tunnel junctions beyond macrospin, Phys. Rev. B **104**, 104428 (2021).

[19] M. I. Dyakonov and V. I. Perel, Current-induced spin orientation of electrons in semiconductors, Phys. Lett. A **35**, 459 (1971).

[20] J. E. Hirsch, Spin Hall effect, Phys. Rev. Lett. **83**, 1834 (1999).

[21] S. Zhang, Spin Hall effect in the presence of spin diffusion, Phys. Rev. Lett. **85**, 393 (2000).

[22] S. Takahashi and S. Maekawa, Spin current in metals and superconductors, J. Phys. Soc. Jpn. **77**, 031009 (2008).

[23] C.-F. Pai, L. Liu, Y. Li, H. W. Tseng, D. C. Ralph, and R. A. Buhrman, Spin transfer torque devices utilizing the giant spin Hall effect of tungsten, Appl. Phys. Lett. **101**, 122404 (2012).

[24] A. Hoffmann, Spin Hall effects in metals, IEEE Trans. Magn. **49**, 5172 (2013).

[25] Y.-C. Lau and M. Hayashi, Spin torque efficiency of Ta, W, and Pt in metallic bilayers evaluated by harmonic Hall and spin Hall magnetoresistance measurements, Jpn. J. Appl. Phys. **56**, 0802B5 (2017).

[26] Y. Shiokawa, E. Komura, Y. Ishitani, A. Tsumita, K. Suda, K. Hamanaka, T. Taniguchi, and T. Sasaki, Dependency of high-speed write properties on external magnetic field in spin-orbit torque in-plane magnetoresistance devices, Appl. Phys. Express **14**, 013001 (2021).

[27] J. C. Slonczewski, Current-driven excitation of magnetic multi-layers, J. Magn. Magn. Mater. **159**, L1 (1996).

[28] J. Z. Sun, Spin-current interaction with a monodomain magnetic body: A model study, Phys. Rev. B **62**, 570 (2000).

[29] T. Taniguchi, K. Yamada, and Y. Nakatani, Critical current formula of perpendicularly magnetized magnetic random access memory revisited, Jpn. J. Appl. Phys. **58**, 058001 (2019).

[30] K.-S. Lee, S.-W. Lee, B.-C. Min, and K.-J. Lee, Theoretical current for switching of a perpendicular magnetic layer induced by spin Hall effect, Appl. Phys. Lett. **102**, 112410 (2013).

[31] H. Morise and S. Nakamura, Relaxing-precessional magnetization switching, J. Magn. Magn. Mater. **306**, 260 (2006).

[32] M. Oogane, T. Wakitani, S. Yakata, R. Yilgin, Y. Ando, A. Sakuma, and T. Miyazaki, Magnetic damping in ferromagnetic thin films, Jpn. J. Appl. Phys. **45**, 3889 (2006).

[33] W. F. Brown, Jr., Thermal fluctuations of a single-domain particle, Phys. Rev. **130**, 1677 (1963).

[34] T. Taniguchi, S. Isogami, Y. Shiokawa, Y. Ishitani, E. Komura, T. Sasaki, S. Mitani, and M. Hayashi, Magnetization switching probability in the dynamical switching regime driven by spin-transfer torque, Phys. Rev. B **106**, 104431 (2022).

[35] A. V. Khvalkovskiy, D. Apalkov, S. Watts, R. Chepulskii, R. S. Beach, A. Ong, X. Tang, A. Driskill-Smith, W. H. Butler, P. B. Visscher, D. Lottis, E. Chen, V. Nikitin, and M. Krounbi, Basic principles of STT-MRAM cell operation in memory arrays, J. Phys. D **46**, 074001 (2013).

[36] D. Apalkov, B. Dieny, and J. M. Slaughter, Magnetoresistive random access memory, Proc. IEEE **104**, 1796 (2016).

[37] *Introduction to Magnetic Random-Access Memory*, edited by B. Dieny, R. B. Goldfarb, and K.-J. Lee (Wiley, Hoboken, NJ, 2016).